Parallel computing of wave propagation in three dimensional functionally graded media

Kyoungsoo Park[a], Glaucio H. Paulino[b],*

[a] *School of Civil & Environmental Engineering, Yonsei University, 134 Sinchon-dong, Seodaemun-gu, Seoul, Republic of Korea*
[b] *Department of Civil & Environmental Engineering, University of Illinois at Urbana-Champaign, 205 North Mathews Ave., Urbana, IL 61801, United States*

ARTICLE INFO

ABSTRACT

Parallel computing techniques are employed to investigate wave propagation in three-dimensional functionally graded media. In order to obtain effective and efficient parallel finite element mesh representation, a topology-based data structure (TopS) and a parallel framework for unstructured mesh (ParFUM) are integrated. The parallel computing framework is verified by solving a cantilever example, while the Rayleigh wave speed in functionally graded media is investigated by comparing the results with the homogeneous case. The computational results illustrate that when the elastic modulus of a graded media increase along the depth direction, the Rayleigh wave speed of a graded media is higher than the speed of a homogeneous media with the same material properties on the surface.

© 2011 Elsevier Ltd. All rights reserved.

1. Introduction

Natural and engineered materials may display spatial variation of microstructure to improve performance such as hardness, toughness, thermal resistance, corrosion resistance, etc. (Paulino, 2002). These materials are named as functionally graded materials (FGMs). For example, bamboo has an optimized microstructure that corresponds to the concept of FGMs. In order to achieve high performance in both thermal and mechanical resistances for thermal protection structures, one phase of a microstructure can be ceramic that provides heat and corrosion resistance, while the other phase can be metallic that leads to high strength and toughness. Moreover, in order to obtain an efficient and multifunctional concrete structure, fiber volume fraction can spatially vary within a structure.

Because of their promising high performances, dynamic responses of FGMs have been invested by many researchers. For instance, Praveen and Reddy (1998) studied functionally graded plate whose material properties vary along the thickness direction, and demonstrated that the gradients in material properties significantly influence the response of FGM plates. Han and Liu (2002) utilized quadratic layer element to analyze SH waves in FGM plates. Based on the elastic wave theory, Li et al. (2004) investigated Love waves in a functionally graded piezoelectric material layer. Zhang

and Paulino (2007) presented the effect of material gradation on characteristics of wave propagation and stress redistribution of FGMs. Recently, Anandakumar and Kim (2010) performed a modal analysis of a functionally graded cantilever beam.

The present paper focuses on three-dimensional dynamic responses of FGMs by means of parallel computing techniques in order to tackle large-scale problems. Especially, the Rayleigh wave in functionally graded media is of interest to this study. A novel parallel computing framework is developed by integrating a topology based data structure (TopS) and a parallel framework for unstructured mesh (ParFUM). The remaining of the paper is organized as follows. In the next section, a computational framework for the parallel computation of the wave propagation is presented. Section 3 demonstrates the verification and runtime performance of the computational framework, while Section 4 investigates three-dimensional wave propagation in functionally graded media. Finally, concluding remarks are provided in Section 5.

2. Basic computational framework

A governing equation of the Galerkin finite element formulation is obtained from the principle of the virtual work. The summation of the virtual strain energy and the virtual kinetic energy is equal to the virtual work done by the external traction ($\mathbf{T}^{ext}$):

$$\int_{\Omega} \left(\delta\boldsymbol{\varepsilon} : \boldsymbol{\sigma} + \delta\mathbf{u} \cdot \rho\ddot{\mathbf{u}} \right) d\Omega = \int_{\Gamma} \delta\mathbf{u} \cdot \mathbf{T}^{ext} \, d\Gamma \qquad (1)$$

* Corresponding author. Tel.: +1 217 333 3817; fax: +1 217 265 8641.
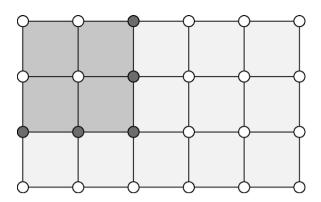 *E-mail address:* paulino@uiuc.edu (G.H. Paulino).

Fig. 1. Illustration of mesh partition, and shared nodes along the mesh partition boundary.

where Ω and Γ are domain and boundary, respectively. Small deformation condition is assumed, and $\boldsymbol{\varepsilon}$ and $\boldsymbol{\sigma}$ are strain and stress tensors, respectively. In addition, $\mathbf{u}$ is a displacement vector, ρ is the density, and the superimposed dot denotes the time derivative. The weak form is discretized into finite elements, which leads to the following equation of motion, i.e. $\mathbf{M\ddot{u}}_n + \mathbf{Ku}_n = \mathbf{F}^{ext}$, where $\mathbf{M}$ and $\mathbf{K}$ are the mass matrix and the stiffness matrix, respectively, and $\mathbf{F}^{ext}$ is the external force vector. Additionally, $\mathbf{\ddot{u}}_n$ and $\mathbf{u}_n$ are nodal acceleration and displacement vectors at time n, respectively. The equation of motion is solved by employing the central difference method, i.e. explicit time integration (Newmark, 1959). The nodal displacement ($\mathbf{u}_{n+1}$), velocity ($\mathbf{\dot{u}}_{n+1}$) and acceleration ($\mathbf{\ddot{u}}_{n+1}$) at time $n+1$ are approximated as:

$$\mathbf{u}_{n+1} = \mathbf{u}_n + \Delta t \mathbf{\dot{u}}_n + \frac{\Delta t^2}{2} \mathbf{\ddot{u}}_n \tag{2}$$

$$\mathbf{\dot{u}}_{n+1} = \mathbf{\dot{u}}_n + \frac{\Delta t}{2} (\mathbf{\ddot{u}}_n + \mathbf{\ddot{u}}_{n+1}) \tag{3}$$

$$\mathbf{\ddot{u}}_{n+1} = \mathbf{M}^{-1} (\mathbf{F}^{ext}_{n+1} - \mathbf{F}^{int}_{n+1}) \tag{4}$$

where $\mathbf{F}^{int}$ is the internal force vector. Note that one does not need to solve a linear system of equations if one utilizes a lumped mass matrix, i.e. diagonal matrix. In the current study, a lumped mass matrix is obtained by considering diagonal terms of the consistent mass matrix and scaling them to preserve the total mass (Hughes, 2000).

In parallel computing, the time integration algorithm requires communications between partitioned meshes because the evaluation of nodal accelerations needs adjacent element information. In order to obtain adjacent element information, the concept of a sum over shared nodes (Lawlor et al., 2006) is utilized. For example, a finite element mesh is decomposed into two chunk of meshes: one chunk with dark gray elements and the other chunk with light gray elements, as shown in Fig. 1. Shared nodes are defined along the partitioned mesh boundary, as described in dark gray nodes. The internal force at shared nodes is obtained by adding the inter-

nal forces of adjacent elements. In this case, the communication between partitioned meshes is needed because adjacent elements are not in the same mesh partition. Note that nodal accelerations of white nodes are evaluated locally because all the adjacent elements are within the same mesh partition. Moreover, all nodal displacements and velocities are obtained locally, and thus the communication is not needed for the evaluation of nodal displacements and velocities.

The parallel finite element analysis framework is implemented by means of TopS and ParFUM. TopS is a topology based data structure, and provides compact and complete topological information such as *node*, *element*, *vertex*, *edge* and *facet* for finite element mesh representation (Celes et al., 2005a; Paulino et al., 2008). Note that *node* and *element* are explicitly represented while *vertex*, *edge* and *facet* are implicitly represented by using *concrete types* (Celes et al., 2005b). ParFUM is a parallel programing framework for scalable engineering applications like the finite element analysis (Lawlor et al., 2006). It supports parallel communications between partitioned meshes through introducing ghosts and shared nodes. Note that ParFUM is built on top of a parallel programing interface, named as CHARM++, which provides capabilities such as dynamic load balancing, automatic check-pointing, communication optimization and processor virtualization (Kale and Krishnan, 1996; Kale and Zheng, 2009; Lawlor et al., 2006). Instead of integrating TopS and ParFUM, one can alternatively employ a parallel topology based data structure, called ParTopS, for a parallel finite element mesh representation (Espinha et al., 2009).

For the consideration of functionally graded media, the generalized isoparametric formulation (GIF) (Kim and Paulino, 2002) is utilized. Material properties at integration points are interpolated from the nodal quantities by using the same shape functions as the geometric and displacement representation (i.e. isoparametric). For example, the elastic modulus and density at the numerical integration points are evaluated as:

$$E = \sum_{i=1}^{n_{el}} N_i E_i, \quad \rho = \sum_{i=1}^{n_{el}} N_i \rho_i \tag{5}$$

where n_{el} is the number of nodes in an element, N_i are the Lagrange basis shape functions, and E_i and ρ_i are elastic modulus and density at nodal locations. The GIF approach reduces stress discontinuity, and generally provides more accurate stress distributions in graded media. In addition, Santare et al. (2003) compared the conventional elements approach (i.e. material properties are constant within an element) to the graded element approach, and demonstrated that the graded element approach generally provided a smoother stress field for dynamic problems.

Additionally, the domain decomposition is performed by using a software package, i.e. METIS, whose algorithms are based on multilevel graph partitioning (Karypis and Kumar, 1998a,b). For the visualization of large scale data, the Parallel Visualization Application, i.e. ParaView (Squillacote, 2006), can be utilized.
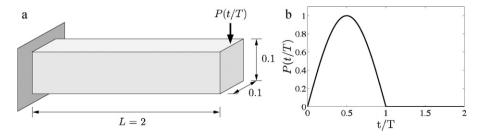

Fig. 2. (a) Geometry of a cantilever and (b) applied sinusoidal transient force, $P(t/T)$.
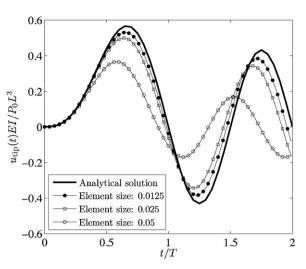
Fig. 3. Convergence of computational results to the analytical solution under the mesh refinement.
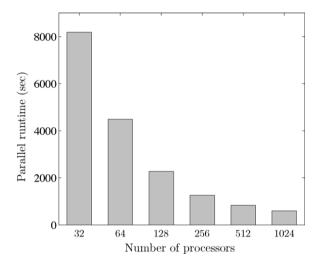

Fig. 4. Parallel runtime performance with respect to the number of processors.

3. Verification and runtime performance

The parallel computational framework is verified by solving a cantilever example, and its parallel runtime performance is presented. The geometry of a cantilever is shown in Fig. 2(a), and a sinusoidal transient load ($P(t/T) = P_0 \sin(\pi t/T)$) is applied at the tip of the cantilever, as shown in Fig. 2(b), where t and T are time and period, respectively. The problem has an analytical solution,

Table 1
Elastic material properties of the homogeneous media.

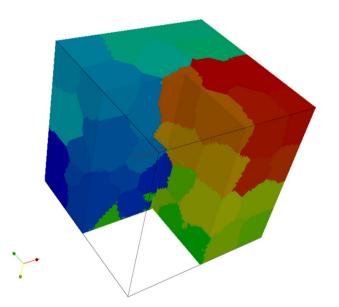|	C_P (km/s)	C_S (km/s)	ρ (kg/m^3)	E (GPa)	ν
Homogeneous	2	1.2	2	7.02	0.219

Fig. 6. Illustration of a partitioned finite element mesh (domain decomposition).

given by Warburton (1976). For $0 \le t \le T$, the tip displacement of the cantilever (u_{tip}) is expressed as:

$$u_{\text{tip}}(t) = \frac{4P_0}{m} \sum_i \frac{1}{\omega_i} \int_0^t \sin\frac{\pi\tau}{T} \sin\omega_i(t - \tau)\, d\tau \qquad (6)$$

where m is the total mass, and ω_i are natural frequencies. When t is greater than T, i.e. $t > T$, the external transient load is zero, and thus the response corresponds to the free vibration in this example. The tip displacement is given as:

$$u_{\text{tip}}(t) = \frac{4P_0 L^3}{EI} \sum_i \frac{\pi\omega_i T}{(\lambda_i L)^4(\pi^2 - (\omega_i T)^2)} \left\{ \sin\omega_i(t - T) + \sin\omega_i t \right\}$$

$$(7)$$

where E is the elastic modulus, I is the second moment of cross-sectional area, and λ_i is a dimensional parameter. Note that the natural frequencies (ω_i) are expressed as $\lambda_i^2 \sqrt{EI/m}$; and λ_i are the successive roots of the frequency equation, i.e. $\cos\lambda L \cosh\lambda L + 1 = 0$. The roots are given as $\lambda_1 L = 1.875$, $\lambda_2 L = 4.694$, $\lambda_3 L = 7.855$ and $\lambda_i L \simeq (i - 0.5)\pi$ for $i \ge 4$.
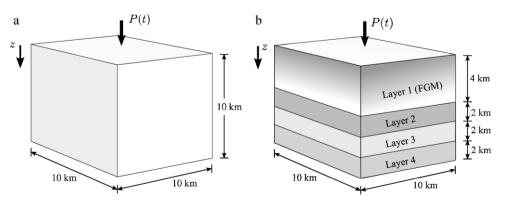

Fig. 5. Geological system: (a) homogeneous media and (b) functionally graded media.
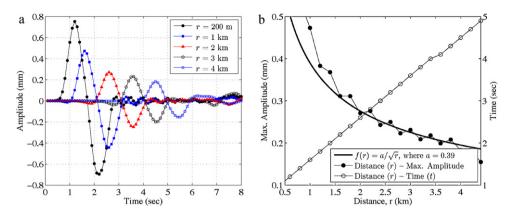
Fig. 7. Dynamic responses of the homogeneous case: (a) vertical displacement amplitude versus time and (b) distance from the source versus the maximum displacement amplitude and corresponding time.

Table 2
Elastic material properties of the functionally graded media.

	C_P (km/s)	C_S (km/s)	ρ (kg/m^3)	E (GPa)	ν
Graded layer 1	2/3.6	1.2/2.16	2/3.6	7.02/40.94	0.219/0.219
Layer 2	3.5	2.1	2.3	24.7	0.336
Layer 3	4.5	2.1	2.3	27.6	0.361
Layer 4	5.5	2.1	2.3	28.7	0.430

The cantilever domain is discretized into linear tetrahedral elements (Tet4), with $2 \times 2 \times 40$, $4 \times 4 \times 80$, and $8 \times 8 \times 160$ mesh grids, which lead to the element size of 0.05, 0.025 and 0.0125, respectively. The numbers of nodes are 369, 2025 and 92769, and the numbers of elements are 800, 6400 and 409600 for each discretization. The tip displacement (u_{tip}) versus time t curves are plotted in Fig. 3. Computational results converge to the analytical solution under the mesh refinement.

For the estimation of the parallel runtime performance, Intel 64 Cluster Abe is utilized, which is located at the National Center for Supercomputing Applications (NCSA) at the University of Illinois at Urbana-Champaign. The peak floating point operations per second (FLOPS) is 89.47 TF, the processor is Intel 64 2.33 GHz dual socket quad core, and each core has 1 GB memory. The finite element mesh with the $8 \times 8 \times 160$ grid is decomposed into 32, 64, 128, 256, 512 and 1024 domains, and each domain has 12800, 6400, 3200, 1600, 800 and 400 tetrahedral elements, respectively. Each domain is assigned into each processor, and the parallel runtime is plotted in Fig. 4. The runtime decreases almost in a half up to the use of 512 processors while the number of processors doubles in this example. When the number of elements in each processor is small, which corresponds to the case of 1024 decomposed domain, the parallel efficiency decreases, as expected.

4. Three-dimensional geology simulation

In this section, dynamic responses and the Rayleigh wave speed are investigated in a geological system. Note that Rayleigh waves were first found by Rayleigh (1885); the Rayleigh wave velocity is related to material properties such as density, elastic modulus and Poisson's ratio. Because of its importance, Rayleigh waves have been utilized to investigate in many research areas such as seismology, geology, material science, etc. (Fourney and Rossmanith, 1980; Cielo et al., 1985; Snieder, 1988; Simons et al., 1999).

A geological domain is considered as a $10\,\text{km} \times 10\,\text{km} \times 10\,\text{km}$ hexahedron (Fig. 5). A point source is applied at the center of the top surface with a sinusoidal transient load, i.e. $P(t) = \sin(\pi t/2)$, for 2 seconds. Two examples are investigated: one with a homo-

geneous media, and the other with a graded media, as shown in Fig. 5(a) and (b), respectively. The domain is discretized into a $50 \times 50 \times 50$ mesh grid with linear tetrahedral elements. The number of nodes is 132651, and the number of elements is 625000. Each color in Fig. 6 illustrates the chunk of meshes assigned to each processor.

The homogeneous example (Fig. 5(a)) is first investigated, and its material properties are illustrated in Table 1. The displacement amplitude at the distance (r) from the source point is observed on the top surface ($z = 0$). Fig. 7(a) illustrates the time versus the vertical displacement curves with respect to the distance from the source point, i.e. $r = 200\,\text{m}$, 1 km, 2 km, 3 km and 4 km. The increase of r leads to the longer time for the wave to arrive and the decrease of the vertical displacement amplitude. In addition, the distance (r) versus the maximum amplitude relation is plotted in the solid-circle line in Fig. 7(b). The maximum amplitude decreases in the proportion of the square root of the distance (r), which corresponds to the solid line. The distance (r) versus the time at the maximum amplitude is also plotted in the white-circle line. The slope of the white-circle line (i.e. distance versus time) represents the inverse of the Rayleigh wave speed obtained from the numerical simulation. The inverse of the slope is approximately 1 km/s, which corresponds to the theoretical value of the Rayleigh wave speed ($C_R = 1.1\,\text{km}$) in the homogeneous media.

Next, the functionally graded domain is investigated, shown in Fig. 5(b). The domain consists of four layers: one graded layer and three homogeneous layers. The material properties of each layer are summarized in Table 2 (Pereyra et al., 1992). In the graded layer, the elastic modulus and Poisson's ratio vary linearly along the depth direction. Note that the material properties on the surface are the same as the material properties of the previous (homogeneous) example. However, the elastic modulus of the top layer increases from 7 GPa to 40 GPa with respect to the increase of the depth.

The vertical displacement on the top surface with respect to time is plotted in Fig. 8(a). Because of the material gradation, Fig. 8(a) illustrates that the maximum amplitudes are lower than those in Fig. 7(a). Similarly, in Fig. 8(b), the maximum amplitude versus distance (r) is plotted in the solid-circle line. Two functions are
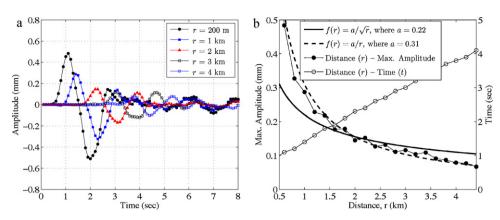
Fig. 8. Dynamic responses of the functionally graded case: (a) vertical displacement amplitude versus time and (b) distance from the source versus the maximum displacement amplitude and corresponding time.

also plotted in solid and dashed lines, which are inverse proportional to $\sqrt{r}$ and r, respectively. Note that, in the graded media, the maximum amplitude is not proportional to the one over square root r, but it is in-between $1/r$ and $1/\sqrt{r}$ for this example. The distance (r) versus the time at the maximum amplitude is also plotted in the white-circle line. The computed Rayleigh wave speed (i.e. inverse of the slope) is 1.25 km/s, which is higher than the homogeneous media although the surface material properties of the graded media are the same as the material properties of the homogeneous case. This is because Rayleigh waves are associated with surface movements within a shallow depth. Thus, the change of the elastic modulus within a shallow depth influences the Rayleigh wave speed. For example, when the elastic modulus increases along the depth direction, the Rayleigh wave speed increases because, in general, the higher the elastic modulus, the faster the Rayleigh wave speed.

5. Concluding remarks

The Rayleigh wave speed in functionally graded media is investigated. Three-dimensional computational results illustrate that the Rayleigh speed in a graded media is different from the speed in a homogeneous media with the same material properties on the surface. In order to tackle large scale problems, a parallel computation framework is developed by integrating TopS and ParFUM. The computational framework is verified by solving a cantilever example, while the parallel runtime performance is estimated in order to demonstrate a potential scalability of the parallel computation framework. Furthermore, the research will be extended to investigate nonlinear dynamic crack propagation problems by using the cohesive zone modeling.

Appendix A. Appendix

A brief explanation on acronyms (i.e. TopS, ParFUM, CHARM++, ParTopS, METIS, ParaView) is provided in Table A.1. For more detailed information associated with implementation and algorithms, one may read the corresponding references.

Table A.1
Description of acronyms associated with parallel computational frameworks.

Acronyms	Description	References
TopS	• A topology based data structure for an efficient finite element mesh representation • The data structure provides compact and complete topological information such as *node*, *element*, *vertex*, *edge* and *facet* • *Node* and *element* are explicitly represented, while *vertex*, *edge* and *facet* are implicitly represented by using *concrete types*	Celes et al. (2005a,b); Paulino et al. (2008)
ParFUM	• A parallel programing framework for engineering applications (e.g. finite element analysis) • Communications between partitioned meshes are performed by introducing ghosts and shared nodes • ParFUM is built on top of CHARM++	Lawlor et al. (2006)
Charm++	• A parallel programing interface • The interface supports capabilities including dynamic load balancing, automatic check-pointing, communication optimization, and processor virtualization	Kale and Krishnan (1996); Kale and Zheng (2009)
ParTopS	• A topology based data structure for a parallel finite element mesh representation	Espinha et al. (2009)
METIS	• A domain decomposition package based on multilevel graph partitioning algorithms	Karypis and Kumar (1998a,b)
ParaView	• A visualization software for large scale data	Squillacote (2006)

References

Anandakumar, G., Kim, J.-H., 2010. On the modal behavior of a three-dimensional functionally graded cantilever beam: Poisson's ratio and material sampling effects. Composite Structures 92 (6), 1358–1371.

Celes, W., Paulino, G.H., Espinha, R., 2005a. A compact adjacency-based topological data structure for finite element mesh representation. International Journal for Numerical Methods in Engineering 64 (11), 1529–1556.

Celes, W., Paulino, G.H., Espinha, R., 2005b. Efficient handling of implicit entities in reduced mesh representations. Journal of Computing and Information Science in Engineering 5 (4), 348–359.

Cielo, P., Nadeau, F., Lamontagne, M., 1985. Laser generation of convergent acoustic waves for materials inspection. Ultrasonics 23 (2), 55–62.

Espinha, R., Celes, W., Rodriguez, N., Paulino, G.H., 2009. ParTopS: compact topological framework for parallel fragmentation simulations. Engineering with Computers 25 (4), 345–365.

Fourney, W.L., Rossmanith, H.P., 1980. Crack tip position and speed as determined from Rayleigh wave patterns. Mechanics Research Communications 7 (5), 277–281.

Han, X., Liu, G.R., 2002. Effects of SH waves in a functionally graded plate. Mechanics Research Communications 29 (5), 327–338.

Hughes, T.J.R., 2000. The Finite Element Method: Linear Static and Dynamic Finite Element Analysis. Dover Publications, New York.

Kale, L.V., Krishnan, S. (1996). Parallel Programming Using C++. MIT Press, Cambridge, pp. 175–213, Ch. 5 CHARM++: Parallel Programming with Message-Driven Objects.

Kale, L.V., Zheng, G. (2009). Advanced Computational Infrastructures for Parallel and Distributed Applications. John Wiley & Sons, pp. 265–282, Ch. 13 Charm++ and AMPI: Adaptive Runtime Strategies via Migratable Objects.

Karypis, G., Kumar, V., 1998a. A fast and high quality multilevel scheme for partitioning irregular graphs. SIAM Journal on Scientific Computing 20 (1), 359–392.

Karypis, G., Kumar, V., 1998b. Multilevel k-way partitioning scheme for irregular graphs. Journal of Parallel and Distributed Computing 48 (1), 96–129.

Kim, J.H., Paulino, G.H., 2002. Isoparametric graded finite elements for nonhomogeneous isotropic and orthotropic materials. Journal of Applied Mechanics – Transactions of the ASME 69 (4), 502–514.

Lawlor, O.S., Chakravorty, S., Wilmarth, T.L., Choudhury, N., Dooley, I., Zheng, G., Kale, L.V., 2006. ParFUM: a parallel framework for unstructured meshes for scalable dynamic physics applications. Engineering with Computers 22 (3–4), 215–235.

Li, X.Y., Wang, Z.K., Huang, S.H., 2004. Love waves in functionally graded piezoelectric materials. International Journal of Solids and Structures 41 (26), 7309–7328.

Newmark, N.M., 1959. A method of computation for structural dynamics, Journal of Engineering Mechanics Division. ASCE 85, 67–94.

Paulino, G.H., 2002. Fracture of functionally graded materials. Engineering Fracture Mechanics 69 (14–16), 1519–1520.

Paulino, G.H., Celes, W., Espinha, R., Zhang, Z.J., 2008. A general topology-based framework for adaptive insertion of cohesive elements in finite element meshes. Engineering with Computers 24 (1), 59–78.

Pereyra, V., Richardson, E., Zarantonello, S.E. (1992). Large scale calculations of 3D elastic wave propagation in a complex geology. In: Proceedings, Supercomputing, '92. Los Alamitos, CA, USA, pp. 301–309.

Praveen, G.N., Reddy, J.N., 1998. Nonlinear transient thermoelastic analysis of functionally graded ceramic–metal plates. International Journal of Solids and Structures 35 (33), 4457–4476.

Rayleigh, L., 1885. On waves propagated along the plane surface of an elastic solid. In: Proceedings London Mathematical Society s1-17, vol. 1 , pp. 4–11.

Santare, M.H., Thamburaj, P., Gazonas, G.A., 2003. The use of graded finite elements in the study of elastic wave propagation in continuously nonhomogeneous materials. International Journal of Solids and Structures 40 (21), 5621–5634.

Simons, F.J., Zielhuis, A., van der Hilst, R.D. (1999). The deep structure of the Australian continent from surface wave tomography. In: van der Hilst, R.D., McDonough, W.F. (Eds.), Composition, Deep Structure and Evolution of Continents. Vol. 24 of Developments in Geotectonics. Elsevier, pp. 17–43.

Snieder, R., 1988. Large-scale waveform inversions of surface waves for lateral heterogeneity. 2. Application to surface waves in Europe and the Mediterranean. Journal of Geophysical Research 93 (B10), 12067–12080.

Squillacote, A.H., 2006. ParaView Guide: A Parallel Visualization Application. Kitware, Inc.

Warburton, G.B., 1976. The Dynamical Behaviour of Structures. Pergamon Press, Oxford, UK.

Zhang, Z., Paulino, G.H., 2007. Wave propagation and dynamic analysis of smoothly graded heterogeneous continua using graded finite elements. International Journal of Solids and Structures 44 (11–12), 3601–3626.